Journal of Sol-Gel Science and Technology
https://doi.org/10.1007/s10971-022-05988-6

ORIGINAL PAPER: INDUSTRIAL AND TECHNOLOGICAL APPLICATIONS OF SOL–GEL AND HYBRID MATERIALS

Industrial applications of sol–gel derived coatings

Songwei Lu[1] · Jiping Shao[2] · Fanghui Wu[2]

Received: 26 August 2022 / Accepted: 2 November 2022

Abstract

Sol–gel derived coatings have many practical applications in different industries. In this paper, HI-GARD® hard coat, multi-layer antireflective coatings, and an anti-glare coating with organic particles are described. Optical and mechanical performances of these coatings are discussed in addition to adhesion properties. The HI-GARD® hard coat was dip or spin coated from a sol by hydrolyzing alkoxysilanes with water in an acidic condition. The hard coat acts as a protective coating for optical lenses with excellent optical properties with a Bayer ratio of 4.8 and an adhesion of 5B. The multi-layer antireflective coatings were prepared by incorporating titanium oxide sol into the HI-GARD® hard coat solution to obtain different layers by spin-coating with tunable refractive index. These two-layer or three-layer antireflective coatings increase transmittance by at least 3% compared to an uncoated glass substrate. Anti-glare coatings were spray-coated at room temperature on glass substrates by embedding cationic or anionic polystyrene particles in an acid-hydrolyzed silane sol. The anti-glare coating with organic particles can provide a significant glare reduction with a haze value of up to 13% for display surface without sparkling. In addition to these transparent coatings, non-transparent sol–gel derived coatings such as a sol–gel non-stick coating for cookware and bakeware, and two zinc-silicate protective coatings hydrolyzed from a silane with addition of zinc dusts for corrosion protection are also discussed briefly.

Graphical Abstract

The schematic structures of the hard coat on CR-39® substrate, three-layer AR coatings on glass substrate, and organic particle embedded anti-glare coatings on glass substrate, and their respective transmittance or reflective curves

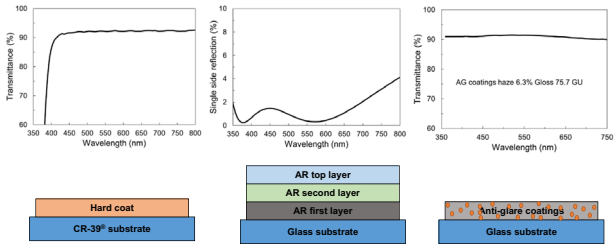

Keywords Hard coat · Antireflective coatings · Multi-layer coatings · Anti-glare coatings · Non-stick coatings · Protective coatings

✉ Songwei Lu
slu@ppg.com

[1] Coatings Innovations Center, PPG Industries, Inc., 4325 Rosanna Drive, Allison Park, PA 15101, USA

[2] Monroeville Business and Technology Center, PPG Industries, Inc., 440 College Park Drive, Monroeville, PA 15146, USA

Published online: 02 December 2022

Highlights

- HI-GARD® hard coat with excellent scratch resistance, optical properties, and adhesion.
- Multi-layer anti-reflective coatings with at least 3% decrease of single side reflectance.
- Anti-glare coatings with organic particles coated at room temperature to reduce glare.

1 Introduction

Sol–gel-derived transparent functional coatings have many industrial applications in recent years due to their superior optical [1–5], mechanical [6, 7], electrical [8], and functional properties [4, 9]. Kajioka et al. achieved low sparkling in anti-glare spray coatings by controlling the size of polymerized species in silica sols with the transmittance haze as high as 12.38% [1]. However, no mechanical durability is reported, which is a requirement for anti-glare coatings on touch screen displays. By adjusting the spray parameters, Huang et al. were able to achieve a sol–gel anti-glare coating with a high haze of 57.0% and a gloss of only 9.2 gloss unit [2]. Wang et al. used a double-layer film to combine the anti-reflective performance with self-cleaning performance using anti-reflective hydrophobic coatings for PV modules [4]. The water contact angle of the surface layer is 150° in the super-hydrophobic state, and the transmittance increases by 5% compared to uncoated glass. Although it is claimed that the coatings have excellent durability, the coating showed scratches with 4H pencil hardness due to its weak surface nanostructures. Zhang et al. prepared ladder-like, cage-like, and/or partial cage-like structures of cycloaliphatic epoxy-functionalized oligosiloxanes (CEOS) by a sol–gel method and incorporated them in a coating followed by a thermal curing [6]. The coating is transparent with a transmittance of 94.9% at 500 nm, flexible, and high pencil harness at 9H on PET substrate. However, in order to get 9H pencil hardness, a thermal curing process of 25 h is necessary which is too long for most production processes. Wu et al. investigated a sol–gel hard coat on polycarbonate substrate concluding that the main factors towards improved pencil scratch resistance are layer thickness, elastic modulus, fracture toughness and intrinsic hardness of the coating material [7]. Pencil hardness is increased from grade 2B to 5H by adjusting these parameters. A good review of sol–gel coatings in the energy sector was recently given by Kaliyanna et al. [10]. Minami reported advanced sol–gel coatings for practical applications including protective coating on metal sheets using methyltrialkoxysilane-derived films, micropatterning on glass substrates, water-repellent coatings for windshields, colored coatings on glass bottles for easy recycling, superhydrophobic and superhydrophilic coatings on glass substrates, and antireflective coatings on glass lenses [11].

Due to the recent work-from-home environment during the COVID-19 pandemic, the needs for smartphones, tablets, and touch screen laptop computers have skyrocketed, as have the needs for transparent functional coatings on these devices. These transparent functional coatings include hard coat, easy-to-clean coatings, anti-glare coatings, antireflective coatings, anti-fingerprint coatings, and anti-static coatings. Besides the optical and functional properties required by these coatings on touch screens, mechanical performance is another requirement that must be met for this application. For example, 9H pencil-hardness hard coating has been applied on plastic substrates for flexible displays [12]. In addition to meet these performance specifications, ease of coating material manufacturing, coating application, and curing are also key requirements for successful practical industrial applications. Furthermore, the use of plastic eyewear substrates has opened a wide door for sol–gel coating application on optical lenses by dip-coating and spin-coating processes. Sol–gel derived hard coat and antireflective coating are common optical coatings in addition to sputtering coatings under vacuum. On the other hand, sol–gel non-transparent coatings have applications in the areas where optical transparency is not a critical factor, e.g., corrosion protection and protective coatings. PPG Industries, Inc. has developed easy-to-clean (EC) coatings for easy-to-clean and silky touch features, along with scratch resistance to protect the uncoated glass substrates; anti-glare (AG) coatings to reduce surface glare to provide better readability under direct light or outdoor without sparkling; antireflective (AR) coatings to reduce surface reflection; and anti-fingerprint (AFP) coatings to reduce fingerprint visibility and better fingerprint cleanability [13]. In this paper, a hard coat on optical lenses, a multi-layer AR coating stack for glass substrates, and an anti-glare coating with organic particles will be described in detail. The non-transparent sol–gel coatings for non-stick coating application, and corrosion protection will also be described briefly.

2 Experimental

2.1 HI-GARD® hard coat

A typical proprietary hard coat solution preparation is described as following: a mixture of alkoxysilanes was added to a suitable vessel such as a 1 L glass flask, and a catalytic amount of an acidic catalyst was added under stirring. Within 10 min, the exotherm generated from the

hydrolysis of the silanes caused an increase in the temperature of the reaction mixture from ~25 to >50 °C. The mixture was stirred for an additional hour while cooling to about 30 °C. A 50/50 weight ratio of alcohol and ether solvents was added to the mixture and stirred. Then an additive, such as polyether-modified polysiloxane copolymer in solvent was added at a low level, and the resulting mixture was stirred for at least 30 min. The resulting coating solution was filtered through a nominal 0.45 µm capsule filter and stored at 4 °C until use.

The hard coat can be easily coated on substrates using standard dip and spin coating processes. A typical application by dip coating is described as following: uncoated optical lenses made of CR-39® monomer or other plastic materials, available from PPG Industries, Inc. were cleaned with different concentrations of caustic cleaning solutions twice under ultrasonics for 5 min for each cleaning. Then the lenses were rinsed with deionized water for three times with each rinse lasting for 5 min before drying at 70–75 °C; the dried lenses were cooled at room temperature for 5 min before the hard coat was applied by a dip-coater. The withdrawal rate used was ~15 cm/min to achieve a cured coating thickness of 3–5 µm. Afterwards, the lenses coated with the hard coat were dried and cured in an air circulating oven for 3 h at 120 °C. Similarly, optical lenses can be coated via spin coating with a spinning speed of 110 rpm, resulting in a coating thickness of ~2–3 µm. The coating can then be cured at 120 °C for 3 h.

2.2 Multi-layer antireflective coatings

2.2.1 Preparation of titanium oxide sol [14]

A sol–gel titanium oxide sol was prepared in a 1 L plastic bottle by slowly adding 440 g of a 6.4% nitric acid aqueous solution to a mixture of 200 g of titanium iso-propoxide (97%, sigma Aldrich), 100 g of DOWANOL™ PM (Propylene glycol mono methyl ether, ≥99.5%, Dow Chemical Company), and 100 g of DOWANOL™ PMA (Propylene glycol methyl ether acetate, ≥99.5%, Dow Chemical Company) under vigorous stirring. White precipitates formed upon adding the acidic solution, and after stirring for 24 h the hydrolyzed solution peptized and became transparent without precipitation or gelation. The titanium oxide sol was stored in a freezer at −20 °C for future use.

2.2.2 Preparation of low refractive index sol–gel solution for a coating with $n = 1.44 \pm 0.01$

The low refractive index sol–gel solution for a coating with $n = 1.44 \pm 0.01$ was prepared using tetraethyl orthosilicate (98% purity, Sigma-Aldrich Corporation), a silane functional acrylic polymer [15] with modification, colloidal silica MT-ST (30 wt% colloidal silica mono-dispersed in methanol, Nissan Chemical), methyltrimthoxysilane (Evonik), 2-propanol, HNO_3, deionized water, and BYK-306 (12.5 wt% polyether-modified polydimethylsiloxane in xylene and monophenyl glycol, BYK USA Inc.). The details of the preparation can be found in Example 5 of referenced patent application [15].

2.2.3 Preparation of sol–gel solutions for sol–gel derived coatings with tunable refractive index

In order to produce multi-layer AR coatings, there should be at least two to three layers with different refractive indices in the final films. It is critical to have appropriate stable sol–gel solutions available. One way to obtain sol–gel films with different refractive indices is to combine one sol–gel solution for high refractive index film with another sol–gel solution for low refractive index film. Figure 1 shows the tunable refractive index of the final films after blending the titanium oxide sol in Section 2.2.1. with a HI-GARD® hard coat sol from PPG Industries, Inc. as mentioned above in Section 2.1. The hard coat sol itself can produce a film with a refractive index of 1.51. Various refractive indices ranging from 1.63 to 1.91 can then be obtained after properly blending by controlling the weight ratio of titanium oxide sol to hard coat sol, thus giving the wider options to design multi-layer AR coatings based on the tunable refractive indices.

2.2.4 Two-layer antireflective (AR) coating stack by spin coating [14]

A soda lime glass substrate was cleaned with isopropyl alcohol and pre-treated with nitrogen plasma treatment for 15 min using an ATTO™ plasma treater (Diener Electronics,

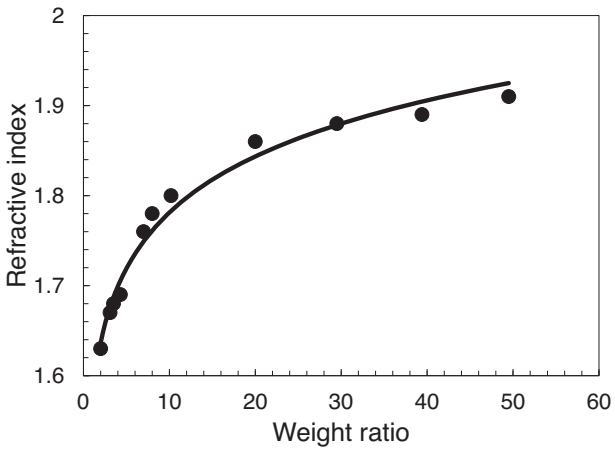

Fig. 1 Tunable refractive index of the final films after blending hard coat sol and titanium oxide sol. The x axis is the weight ratio of titanium oxide sol to the hard coat sol

Germany). The first layer consisting of a coating from the solution for a refractive index of 1.68 ± 0.02 was coated using a Cee™ 200X spin-coater (Cost Effective Equipment, LLC.) on the substrate, followed by curing at 150 °C for 1 h. The film thickness was adjusted by using different spin speeds (500–2000 rpm), and optimal thickness was in the range of 100–140 nm. The second layer consisting of a coating from the solution for a refractive index of 1.44 ± 0.01 was spin coated on top of first layer after nitrogen plasma treatment for 15 min. The thickness of the second layer was in the range of 70 to 90 nm.

2.2.5 Three-layer antireflective (AR) coating stack by spin coating [14]

A soda lime glass substrate was cleaned by isopropyl alcohol, and treated with nitrogen plasma treatment for 15 min using an ATTO™ plasma treater (Diener Electronics, Germany). A coating from the solution for a refractive index of 1.78 ± 0.02 was spin coated on the glass substrate as the first layer. The coating was then dried at 80 °C for 20 min. A second coating from the solution for a refractive index of 1.97 ± 0.03 was spin coated as the second layer followed by drying at 80 °C for 20 min. Thereafter, a coating from the solution for refractive index 1.44 ± 0.01 was coated as the third layer (top layer). The final coating stack was then cured at 150 °C for 1 h. The average film thickness for the first layer, the second layer and the third layer was 50, 83, and 81 nm, respectively.

2.2.6 Anti-glare coatings with particles [16]

Anti-glare coatings solution can be made by incorporating a dispersion of cationic or anionic polystyrene particles in water into the sol–gel matrix. A detailed procedure for preparing a dispersion of cationic or anionic polystyrene particles in water can be found in a granted patent [16]. 30.0 g of tetraethyl orthosilicate (TEOS) from Sigma-Aldrich Corporation, 17.5 g of deionized water, and 17.5 g of denatured ethyl alcohol were mixed together in a flask with a magnetic stirring bar. 1.8 g of 4.68 wt% aqueous nitric acid solution was added to the above mixture to hydrolyze the TEOS. After 1 h stirring, an additional 29.2 g of ethyl alcohol and 4.0 g of cationic or anionic polystyrene particles in water were added to the hydrolyzed sol. The sol was then keep stirring for 10 min.

A glass substrate was treated using a low-pressure plasma system from Diener Electronics, Germany. The above coating solutions were then sprayed on to the glass surface at room temperature using a Spraymation™ and a Binks™ 95 automatic HVLP™ spray gun with a traverse speed of 600 in./min followed by a curing at 150 °C for 1 h.

2.2.7 Coating characterizations

The optical characteristics such as color and % haze of hard coat were measured with a Hunter UltraScan™ PRO. The optical transmittance and reflectance spectra and color of AR coatings were measured using a Lambda™ 9 optical spectrophotometer from 350 to 800 nm. The single side reflection was measured by eliminating the backside reflection by placing a 3M™ black tape on the backside of the sample. The gloss value of the anti-glare-coating coated glass sample was measured using a BYK Gardner™ Micro-Tri-Gloss 20/60/85° gloss meter (BYK-Gardner GmbH, Germany) at 60°. A matte surface of a black paint with a gloss value of <0.5 gloss unit was used under the glass samples to ensure accurate reading. Transmittance, L^*, a^*, b^*, haze, and reflectance of anti-glare coatings were measured using a Color i7 Benchtop Spectrophotometer (X-Rite, Inc., Grand Rapids MI).

The abrasion resistance of hard coat was evaluated via Bayer testing by measuring the haze of both coated and uncoated lenses using a Hunter UltraScan™ PRO after 600 oscillation cycles with 500 g of alundum grits. The Bayer abrasion ratio was calculated using the following formula (Eq. (1)), with the "reference lens" being an uncoated CR-39® as Bayer standard lens.

$$Bayer\ Ratio_{Test\ Lens} = \frac{\left(Haze_{final} - Haze_{initial}\right)_{Avereage\ CR-39\ Refs.}}{\left(Haze_{final} - Haze_{initial}\right)_{Test\ Lens}} \quad (1)$$

The scratch resistance of hard coat was measured using a steel wool test. Optical lenses were subjected to rubbing by selected steel wool under a specified weight, e.g., 1 lb, and a specified number of cycles, e.g., 200 cycles. The haze can be measured before and after rubbing but giving a qualitative rating from poor to excellent is common since the scratches could be localized.

Pencil hardness of anti-glare coatings was measured using an HA-3363 Gardco™ Pencil Scratch Hardness Kit (Paul N. Gardner Company, Inc., Pompano Beach, FL) with a 500 g load and a Derwent graphic pencil. The Erichsen™ hardness of a hybrid non-stick coating was evaluated using an Erichsen™ hardness test pencil model 318S. A dry reciprocating abrasion test was conducted for non-stick coatings to simulate the effect of scraping by spatulas and other cooking utensils. A 2-in. abrasive pad (3M Scotch-Brite 07447) was mounted on a 3 kg armature, which was cycled for 1000. The abrasive pad was replaced with a fresh pad every 1000 cycles, and the test continued until 10% of the abraded area has been exposed to bare metal.

The adhesion of hard coat on substrates can be evaluated with the ASTM D3359 Tape Test or Crosshatch Adhesion Test. First the coated substrate is scored with a crosshatch

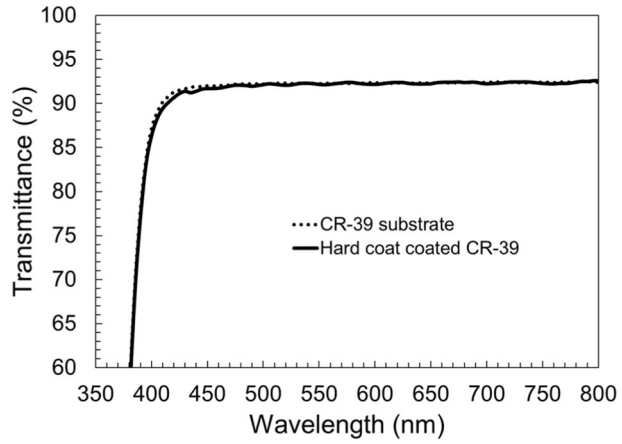

Fig. 2 Transmittance spectra of the hard coat coated CR-39® (solid line) vs uncoated CR-39® substrate (dotted line)

tool twice to form a grid. Then a Scotch™ tape is applied to the grid and quickly removed. For coatings on optical lens, adhesion is evaluated for cured samples at room temperature, and also for the samples submerged in boiling water for 15 min to 3 h. For anti-glare coatings, the crosshatch test was conducted only at room temperature for cured coatings.

Optical profilometry analysis and surface roughness Ra were carried out using a Veeco™ WYKO NT3300 Optical Profilometer. SEM cross-section and top morphology images were taken from a LEO 1530 Field Emission SEM w/ Noran™ EDX System.

3 Results and discussion

3.1 HI-GARD® hard coat performances

3.1.1 Optical performance

The hard coat has excellent optical performances in terms of neutral color, high transmittance, and no haze. Figure 2 shows the transmittance spectra of the hard coat coated CR-39® and uncoated CR-39® substrate. Their spectra are almost identical. The integrated transmittance from 450 nm to 800 nm is about 92% for both coated and uncoated CR-39® substrates. The refractive index of the hard coat of 1.51 matches with that of 1.50 for CR-39® very well. One can also see from Fig. 2 that the CR-39® substrate has significant low transmittance below 380 nm, indicating an excellent UV protection for human eyes. After the coating process, the color data is almost identical to the substrate with slightly higher b^*, which is also confirmed from the yellowness index (YI) with a slightly higher value of 0.76 vs. that of 0.41 for an uncoated CR-39® substrate (Table 1). It is acceptable for vision application with yellowness index as ≤1.0. There is no haze for the coated sample, compared to

Table 1 Optical performance data of the hard coat coated CR-39® vs uncoated CR-39® substrate

Sample	L^*	a^*	b^*	YI	Haze	X	Y	Z
CR-39® substrate	96.92	−0.08	0.26	0.41	0.12	87.41	92.25	98.56
Hard coat coated CR-39®	96.89	−0.15	0.47	0.76	0.03	87.31	92.18	98.21

The optical performance data include L^*, a^*, and b^* from CIBLAB color space, X, Y, Z from CIE 1931 color space, yellow index (YI), and haze

an industrial acceptable standard of less than 0.5% of haze value for optical eyewear applications.

3.1.2 Scratch resistance

The hard coat has not only excellent optical performance, but also excellent mechanical performance to protect the eyewear substrates (Fig. 3). The scratch resistance of the hard coat can be measured with the Bayer test and steel wool test as described in the experimental section. The Bayer test results indicate that the Δ% Haze is 24.0% for the uncoated CR-39® reference lens before and after the Bayer test (Fig. 3a left). The Δ% Haze is only 5.0% for CR-39® lens coated with the hard coat before and after the Bayer test (Fig. 3a right). According to Eq. (1), the Bayer ratio is calculated as 4.8. The steel wool testing results show enhanced scratch resistance when the plastic lens material is protected with the hard coat, with several scratches on the uncoated CR-39® reference lens but no scratches on the hard coat coated CR-39® lens (Fig. 3b). The pencil hardness of the hard coat is 3H. The scratch resistance and pencil hardness are very similar to hard coatings with similar thickness on CR-39® lens prepared based on the nanocomposite of Al_2O_3–ZrO_2 nanoparticles in a sol–gel matrix using 3-glycidoxypropyltrimethoxysilane (GPTMS) and TEOS by Chantarachindawong et al. [5]. However, it seems that the addition of Al_2O_3–ZrO_2 nanoparticles does not show significant benefits for enhancing scratch resistance, e.g., pencil hardness. Only the cracked coating example with 6 μm thickness showed a pencil hardness of >5H [5]. Wu et al. reported that pencil hardness shows continuous improvement to three higher grades with increasing silica content up to 30.5 vol%, but remains stable till 36 vol% silica content [7]. In the current work, the HI-GARD® hard coat has excellent mechanical performance without the addition of alumina, silica, or zirconia nanoparticles.

3.1.3 Hard coat adhesion

The hard coat also has excellent adhesion on CR-39® substrates (Fig. 4). The adhesion on CR-39® substrates is 5B for

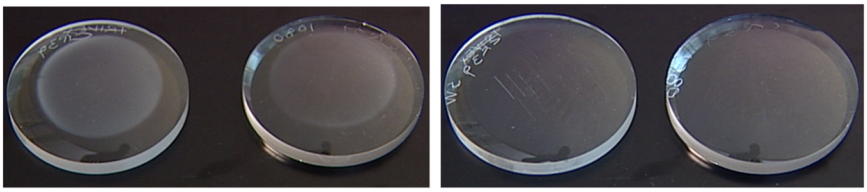

(a) (b)

Fig. 3 Mechanical performance of the hard coat **a** left: uncoated CR-39® reference lens with Δ% Haze = 24.0% before and after Bayer test; and right: CR-39® lens coated with the hard coat with Δ% Haze = 5.0% before and after Bayer test; **b** left: uncoated CR-39® reference lens after scratch testing with steel wool; and right: CR-39® lens coated with the hard coat after scratching testing with steel wool

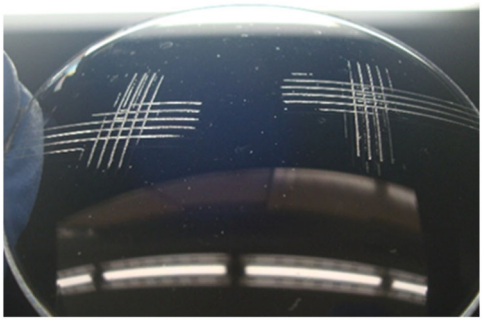

Fig. 4 CR-39® lens coated with the hard coat after cross-hatch adhesion testing with Scotch™ 600 tape showing no coating peeling off after the coated lens was boiled in hot water for 30 min

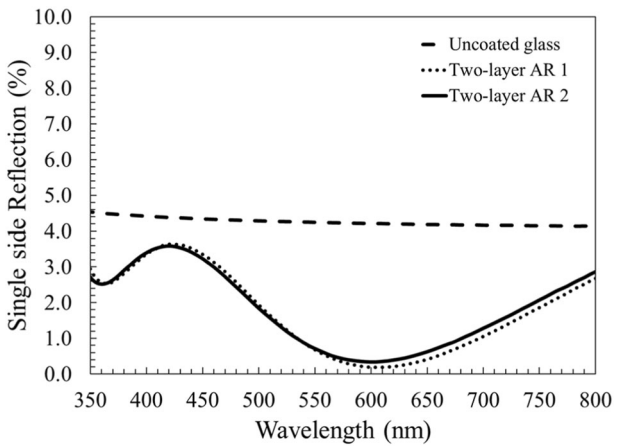

Fig. 5 Single side reflection spectra of two-layer AR coating samples (solid line and dotted line) in comparison with an uncoated glass (dashed line)

samples before and after further boiling water immersion for up to 1 to 3 h.

3.2 Optical performances of two-layer AR coatings

The single side reflection spectra of two samples of two-layer AR coatings are shown in Fig. 5 in comparison to uncoated glass. The reflection curves have a lowest value

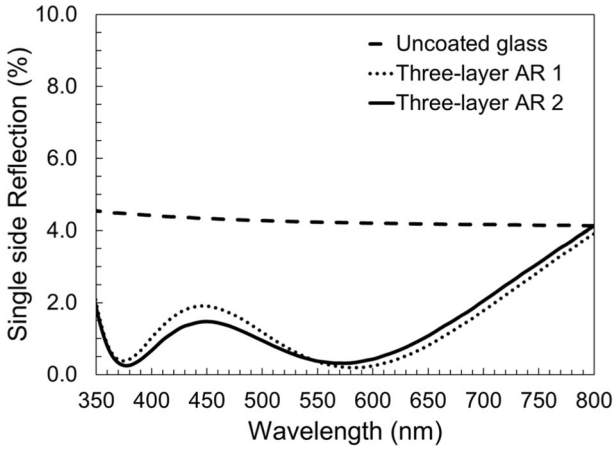

Fig. 6 Single side reflection spectra of three-layer AR coating samples (solid line and dotted line) in comparison with an uncoated glass (dashed line)

around 600 nm. This position of the lowest value can be shifted by adjusting the thickness of each layer. These two samples of two-layer AR coatings have a very slight difference in the reflection curve. Table 2 lists the optical data including color of these two samples in comparison to the uncoated glass. The integrated transmittance of the AR coatings increased by around 3% from the uncoated glass, which is corresponding to the decrease of front reflection by a similar value. The transmittance color of the AR coatings is slightly yellowish giving the positive b^* value. In contrast, the reflective color of the AR coatings is slightly blueish giving the significant negative b* value.

3.3 Optical performances of three-layer AR coatings

The single side reflection spectra of two samples of three-layer AR coatings are shown in Fig. 6 in comparison to the uncoated glass. Comparing to two-layer AR coatings, the spectra show two valleys, with one located in the 370–380 nm range while the second one is located in the 570–590 nm range. The curve forms a W-shape for three-layer AR coatings (Fig. 6), while it is more a V-shaped for

Table 2 Optical performance data of two-layer AR coating samples in comparison with an uncoated glass

Sample name	*T* (%)	Single side R (%)	Front R (%)	Back R (%)	*T*			Front R		
					*L**	*a**	*b**	*L**	*a**	*b**
Uncoated glass	91.83	4.24	8.12	8.12	96.75	−0.03	0.14	34.26	−0.09	−0.59
Two-layer AR 1	94.85	0.95	4.97	5.00	97.93	0.03	1.53	27.00	−0.08	−9.18
Two-layer AR 2	94.84	0.98	5.01	4.99	97.92	−0.07	1.36	27.09	0.38	−8.69

Table 3 Optical performance data of three-layer AR coating samples in comparison with an uncoated glass

Sample name	*T* (%)	Single side R (%)	Front R (%)	Back R (%)	T			Front R		
					*L**	*a**	*b**	*L**	*a**	*b**
Uncoated glass	91.88	4.23	8.11	8.12	96.77	−0.05	0.15	34.23	−0.06	−0.60
Three-layer AR 1	95.17	0.60	4.71	4.73	98.07	−0.05	0.72	26.09	0.39	−5.40
Three-layer AR 2	95.20	0.59	4.73	4.72	98.10	−0.22	0.53	26.08	0.80	−3.72

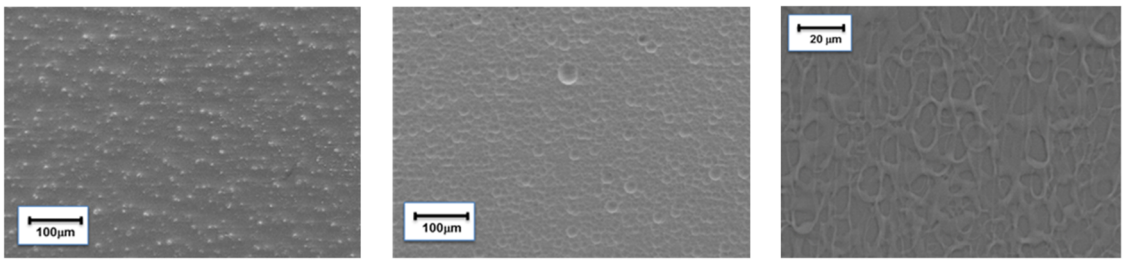

Fig. 7 SEM images of a commercially available anti-glare film (**a**), an anti-glare glass substrate by etching process (**b**), and an anti-glare coating by sol–gel spray process (**c**)

two-layer AR coatings (Fig. 5). The W shape can be changed and the valley locations can be shifted by adjusting the thickness of each layer. Table 3 lists the optical performance data of these three-layer AR coatings. It can be seen that these three-layer AR coatings have slightly higher transmittance, and lower reflectance than the two-layer AR coatings. The three-layer AR coatings may be further optimized to reduce the single side reflection to less than 0.5% or even 0.3%. For these two particular three-layer AR coating samples, their transmittance color is neutral due to *b** value of less than 1, while their reflective color is slightly blue due to slightly negative *b** value (Table 3).

3.4 Antiglare coatings performances

Traditionally, the anti-glare display surface can be formed from an anti-glare film from 3M™ for plastic substrates, or etched glass surface in the case of glass substrates. An anti-glare film may have weak scratch resistance and low pencil hardness on plastic substrates. The etched glass has significant environmental issues using hydrofluoric acid or similar acid as etchant. The by-products during the glass etching process include hexafluorosilicic acid (H_2SiF_6) which can release hydrogen fluoride when evaporated, posing further environmental, health, and safety concerns. On the other hand, anti-glare coatings using the sol–gel process do not generate harmful hydrogen fluoride gas. Figure 7 shows the SEM surface morphologies of three commercial anti-glare surfaces (a) anti-glare film, (b) anti-glare surface by etching process, and (c) anti-glare coatings from PPG Industries, Inc. [13] While the surface morphologies of these samples are all different with (a) consisting of particles, (b) bowl-shaped dents, and (c) random hills and valleys, the principle of the anti-glare surface is the same as using roughed surface features to scatter the light, resulting in significant glare reduction.

The commercially available anti-glare coatings from PPG Industries, Inc. usually require a pre-heated glass substrate [13]. In order to further reduce energy consumption and operational cost for pre-heating process, anti-glare coatings with embedded polystyrene particles have been developed without the pre-heating process.

The cationic or anionic polystyrene particles were first prepared and their dispersion was characterized by high

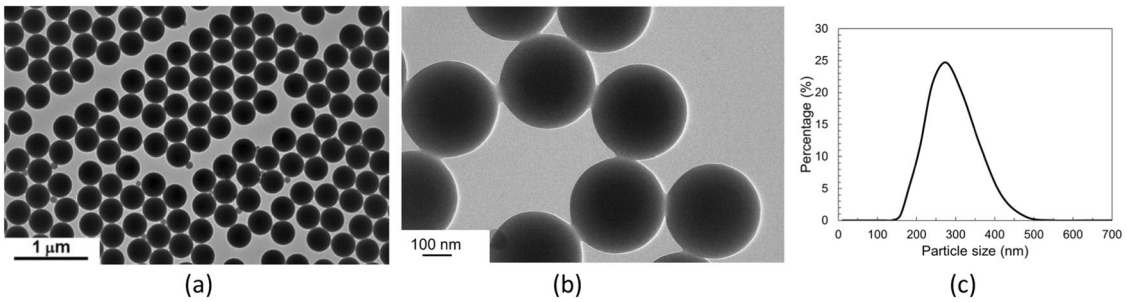

Fig. 8 Typical dispersed cationic or anionic polystyrene particles **a** low magnification, bar 1 μm; **b** high magnification, bar 100 nm, **c** Particle size distribution of typical sample with mean particle size of 292 nm and size ranging from 150 to 500 nm

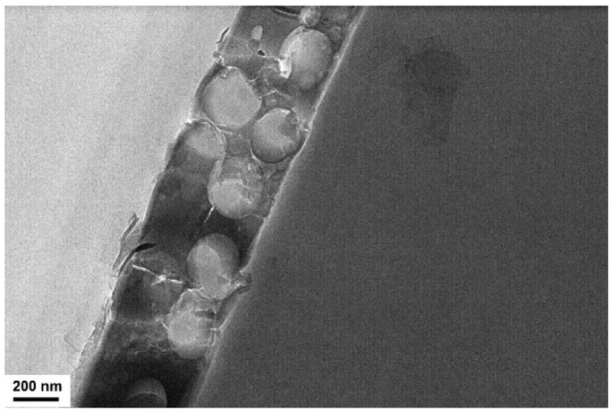

Fig. 9 High resolution TEM cross-sectional image of anti-glare coatings on a Kapton® tape

resolution TEM. Typical dispersed particles are shown in Fig. 8(a) and (b). The mean particle size is 290–300 nm with the particle size ranging from 150 nm to 500 nm (Fig. 8c). When these particles are incorporated in the anti-glare coatings on a Kapton® tape as a substrate, the particles are visible from the cross-sectional HRTEM image (Fig. 9). The surface structure from the anti-glare coatings using particles can be seen in optical profilometry images (Fig. 10). The transmittance curve shown in Fig. 11 indicated that the low haze sample (e.g., haze 6.3%) did not change much of the transmittance curve of the anti-glare coatings, while the high haze sample (e.g., haze 12.2%) has a decrease of about 5% transmittance compared to the uncoated gorilla glass. The haze of 12.2% is comparable with the reported haze of sample S4 from Kajioka et al. [1]; however, the sample in this work has a higher 60° gloss value. The discrepancy could be caused by different structures in the anti-glare coatings, i.e., polystyrene particles vs polymerized species. The haze value is much lower than the reported highest haze of 57.0% [2].

Table 4 lists the optical property, adhesion, and pencil hardness of anti-glare coatings incorporating polystyrene particles. The relationship between haze and 60° gloss value is shown in Fig. 12. When haze decreases, the 60° gloss value increases. Usually, a 70 ± 10 gloss unit will give rise to a 50 ± 10% glare reduction. Depending on the desired extent of the gloss reduction, various 60° gloss values can be obtained by adjusting the spray parameters while still keeping adhesion at 5B and pencil hardness at ≥8H. Due to the roughness of the anti-glare surface, there is a possibility of sparkling from the display with high degree of roughness. Sparkling is a result of the prism effect from the interaction of light from a regular display pixel matrix and anti-glare irregular microstructured surfaces. Displays with higher pixel per inch (PPI) have a higher possibility of sparkling. A higher haze and low gloss anti-glare coating will result in higher possibility of sparkling. Figure 13 illustrates the dependence of sparkling on the surface roughness Ra and PPI, with non-sparkling occurring when Ra is less than 55 nm depending on PPI. This result is contradictory to the conclusion from Kajioka et al.'s work, which indicated that larger polymerized species led to lower gloss, higher haze, and lower sparkle [1]. Sparkling effect wasn't discussed for the highest haze of 57.0% from a sol–gel coating [2].

4 Other industrial applications of sol–gel derived coatings

4.1 Non-stick coatings for cookware and bakeware

A sol–gel-derived non-stick coating for cookware and bakeware has been commercialized using a two-part coating composition [17]. The sol–gel coating composition is based on one or more organoalkoxysilanes such as methyltrimethoxysilane, an acid catalyst for hydrolysis reaction, water, organic polymer particles such as polyphenylene sulfide (PPS), and fillers. The coated panel is then cured above 200 °C, such as at 327 °C for 30 min. When organic polymers are added to the sol–gel precursor mixtures, significant improvements in hardness and abrasion properties can be obtained and preserved up to temperatures close to the melting point, glass-transition temperature, or heat

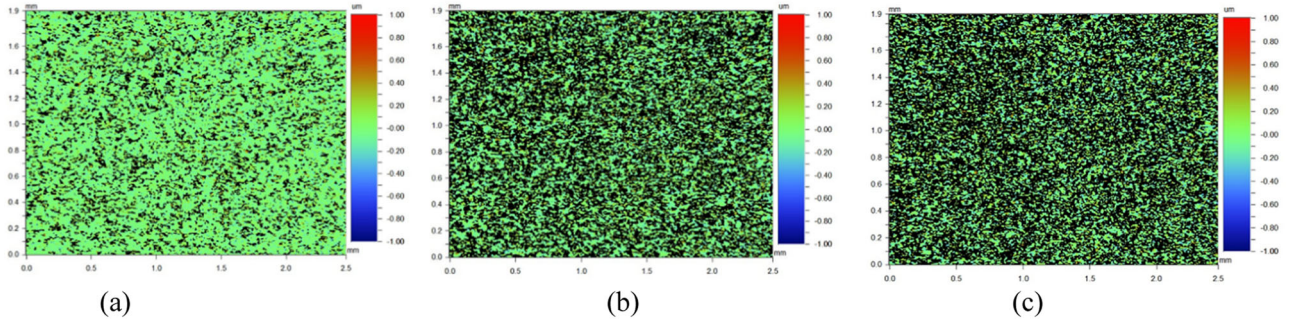

Fig. 10 Optical profilometry images (2.5× magnification) of anti-glare coatings for **a** 73 gloss unit anti-glare coatings with Ra = 77 nm; **b** 61 gloss unit anti-glare coatings with Ra = 106 nm; and **c** 46 gloss unit anti-glare coatings with Ra = 127 nm

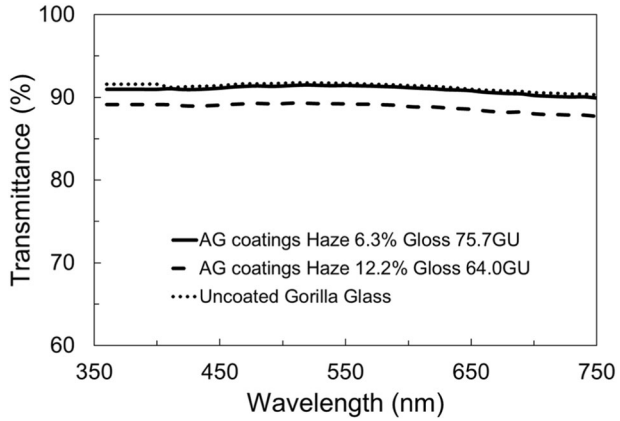

Fig. 11 Transmittance of anti-glare coatings in comparison with the uncoated Gorilla glass substrate

deflection temperature of the chosen polymer. The Fusion™ waterborne sol–gel coatings available from PPG Industries, Inc. is a hybrid organic inorganic coating with good release, stain resistance, and high gloss.

An example of a hybrid coating composition is listed in Table 5 in comparison to a conventional coating composition. The key difference is the addition of polyphenylene sulfide organic particles in the hybrid sol–gel coating composition, which significantly increase the mechanical performances, such as a doubling of the Erichsen™ hardness compared to the conventional composition, and more than a tripling of the performance in the dry reciprocating abrasion test (Table 6).

4.2 Zinc rich sol–gel primer and Aquaweld™ 100 waterborne shop primer

A zinc-rich sol–gel primer is developed for protective and marine coatings, which provides galvanic protection to steel in corrosive environments. The zinc rich primer is based on the hydrolysis of a silane and addition of zinc dusts to form a zinc–silicate matrix for the coatings. After solvent evaporation, the zinc silicate primer is cured by absorption of ambient moisture over 16–24 h. The corrosion protection mechanism is that the steel structure acts as the cathode, while the zinc dust in the primer is the sacrificial metal anode in this electrochemical system. When exposed to an electrolyte such as sea water, the zinc in the primer will corrode preferentially, thus protecting the steel galvanically. In a well-designed coating, the zinc salts that are formed when the zinc corrodes will eventually fill the voids in the zinc primer, and the protection mechanism slowly shifts from galvanic protection to barrier protection. In addition to corrosion resistance, the zinc-silicate coating also has excellent solvent resistance and heat resistance.

A different two-part zinc-silicate waterborne primer called Aquaweld™ 100 has also been developed as a shop primer for pre-construction and pre-fabrication which provides temporary anti-corrosion performance for steel substrates [18]. The two-part sprayable shop primer is an acid stabilized sol–gel coating with addition of zinc dusts and other pigments, forming a moisture curing zinc-silicate network. In general, the shop primer has pot life of about 4 h for application. This red-brown shop primer has good workability through automated spray lines. It has excellent corrosion resistance, cutting properties, and weldability.

5 Summary

PPG Industries Inc. has developed and/or commercialized several sol–gel derived coatings for different applications. The HI-GARD® hard coat has excellent optical and mechanical properties for ophthalmic applications with excellent adhesion on PPG Industries, Inc.'s CR-39®, TRIVEX®, and TRIBRID® substrates and other commercial lens substrates. The hard coat sol can also be blended with a high index titanium oxide sol to form thin films with various refractive indices. Multi-layer antireflective coatings, such as two-layer or three-layer antireflective

Table 4 Optical properties, adhesion, and pencil hardness of anti-glare coatings incorporating polystyrene particles

Sample	Gloss (GU)	Haze (%)	T% at 550 nm	*a**	*b**	*L**	Cross hatch adhesion	Pencil hardness
1	75.7	6.41	91.46	−0.22	0.11	96.56	5B	9H
2	70.0	6.95	91.15	−0.20	0.08	96.45	5B	9H
3	64.7	10.90	89.85	−0.23	−0.03	95.89	5B	9H
4	64.0	11.63	89.75	−0.22	0.02	95.86	5B	9H

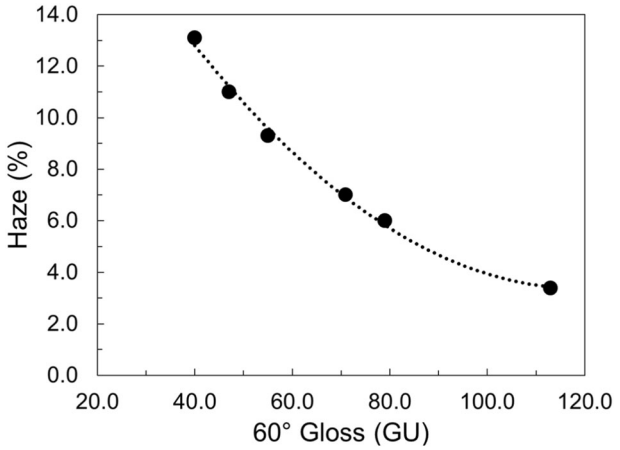

Fig. 12 The relationship of haze vs 60° gloss of the anti-glare coatings

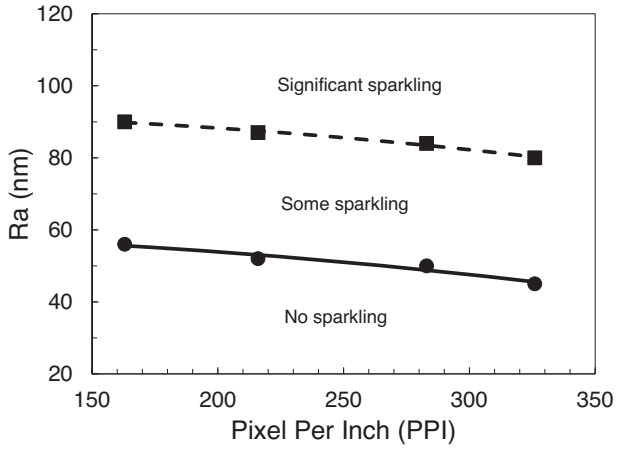

Fig. 13 The dependence of sparkling phenomenon on surface roughness Ra for different display resolutions PPI values

coatings can be spin-coated from coating solutions with desired refractive index on glass substrates. These anti-reflective coatings will have at least 3% increase in transmittance from 350 nm to 800 nm. The anti-glare coatings with cationic or anionic polystyrene particles scatter light to result in a glare reduction without sparkling by controlling the surface roughness Ra. The anti-glare coatings have a crosshatch adhesion of 5B and a pencil hardness of ≥8H. A sol–gel derived non-stick coating has significant improvements in hardness and abrasion properties. Two sol–gel derived zinc-silicate coatings are used as primers on steel substrates to prevent corrosion.

Table 5 Compositional summary of a conventional sol–gel coating and a hybrid sol–gel coating composition for non-stick coatings for cookware and bakeware [18]

Component	Conventional coating composition (wt%)	Hybrid Coating Composition (wt%)
Methyltrimethoxysilane	31.2	33
Silicone fluid	1.16	1.2
Polyphenylene sulfide	0	6.7
Colloidal silica (30%)	43.2	45.2
Black pigments	2.17	2.92
Acid catalyst	0.66	0.7
Pigment dispersant	0.5	1.15
Defoamer	0.58	0.52
Silicon carbide	1	0.98
Dipropylene glycol methyl	6.6	6.4
Other fillers	12.93	1.23
Total	100	100

Table 6 Mechanical performance comparison of conventional sol–gel coating vs. hybrid sol–gel coatings for non-stick coating applications

	Erichsen™ hardness (Newtons)	Dry reciprocating abrasion test (cycles/mil)
Conventional sol–gel coating	8	25,000
Hybrid sol–gel coating	18–20	87,000

Acknowledgements The authors would like to acknowledge experimental results from David C. Martin, Zilu Li, and Xiangling Xu, TEM, SEM, and particle size analyses by PPG Industries, Inc. analytical team, and valuable discussions with Kees Van Vliet, James E. McCarthy, Matteo Sperindio, Vincent Pagnotti, Matthew Luchansky, and Elizabeth Horner, all from PPG Industries, Inc. The authors also would like to thank Michael Buchanan for optical spectrum measurement for antireflective coatings, and Nathaniel Hazelton for optical profilometry measurement for anti-glare coatings, both from Vitro Architectural Glass. Attributions: The *PPG Industries, Inc. Logo*, *CR-39* and *Hi-Gard*, *Trivex* and *Tribrid* are registered trademarks of PPG Industries Ohio, Inc.

Author contributions All authors contributed to part of the experimental and results of the manuscript. The first draft of the manuscript was written by SL and all authors commented on previous versions of the manuscript. All authors read and approved the final manuscript.

Compliance with ethical standards

Conflict of interest The authors declare no competing interests.

References

1. Kajioka T, Kanai T, Ikegami K, Kozuka H (2021) Achievement of low sparkle in anti-glare spray coatings by controlling the size of polymerized species in silica sols. J Sol–Gel Sci Technol 100:244–251
2. Huang YH, Chen LC, Chou HM (2019) Optimization of process parameters for anti-glare spray coating by pressure-feed type automatic air spray gun using response surface methodology. Materials 12:751
3. Abe K, Sanada Y, Morimoto T (2003) Anti-reflective coatings for CRTs by sol–gel process. J Sol–Gel Sci Technol 26:709–713
4. Wang P, Yan X, Zeng J, Luo C, Wang C (2022) Anti-reflective superhydrophobic coatings with excellent durable and self-cleaning properties for solar cells. Appl Surf Sci 602:154408
5. Chantarachindawong R, Osotchan T, Chindaudom P, Srikhirin T (2016) Hard coatings for CR-39 based on Al_2O_3–ZrO_2 3-glycidoxypropyltrimethoxysilane (GPTMS) and tetraethoxysilane (TEOS) nanocomposites. J Sol–Gel Sci Technol 79:190–200
6. Zhang K, Huang S, Wang J, Liu G (2020) Transparent organic/silica nanocomposite coating that is flexible, omniphobic, and harder than a 9H pencil. Chem Eng J 396:125211
7. Wu LYL, Chwa E, Chen Z, Zeng XT (2008) A study towards improving mechanical properties of sol–gel coatings for polycarbonate. Thin Solid Films 516:1056–1062
8. Aegerter MA, Reich A, Ganz D, Gasparro G, Piitz J, Krajewski T (1997) Comparative study of SnO_2:Sb transparent conducting films produced by various coating and heat treatment techniques. J Non-Cryst Solids 218:123–128
9. Esfahani MB, Eshaghi A, Bakhshi SR (2022) Transparent hydrophobic, self-cleaning, anti-icing and anti-dust nano-structured silica based thin film on cover glass solar cell. J Non-Cryst Solids 583:121479
10. Kaliyannan GV, Palanisamy SV, Priyanka EB, Thangavel S, Sivaraj S, Rathanasamy R (2021) Investigation on sol–gel based coatings application in energy sector—a review. Mater Today: Proc 45:1138–1143
11. Minami T (2013) Advanced sol–gel coatings for practical applications. J Sol–Gel Sci Technol 65:4–11
12. Choi GM, Jin J, Shin D, Kim YH, Ko JH, Im HG, Jang J, Jang D, Bae BS (2017) Flexible hard coating: glass-like wear resistant, yet plastic-like compliant, transparent protective coatings for foldable displays. Adv Mater 29:1700205
13. Lu S, Shao J, Martin DC, Li Z, Schwendeman I (2018) Commercialization of sol–gel based transparent functional coatings. J Sol–Gel Sci Technol 87:105–112
14. Lu S, Shao J, Li Z (2019) Multi-layer anti-reflective coated articles. US 2019/0033491 A1
15. Basil JD, Hunia RM, McGrady LB (2013) Polysiloxane coating with hybrid copolymer. US 8,507,631 B2
16. Lu S, Vanier N, Xu X, Martin DC, Olson KG, Schwendeman I (2020) Curable film-forming Sol–gel compositions and anti-glare coated articles formed from them. US 10,723,890 B2
17. Sperindio M, Lake SC, Piras R, Lindstrom MJ (2021) Sol–gel compositions with improved hardness and impact resistance. US 11,193,021 B2
18. Plehiers M, Van Loon S (2013) Binder Composition. US 2013/0289190 A1